

Superconductivity in Bi based Bi_2PdPt

A. Kataria,¹ T. Agarwal,¹ S. Sharma,¹ D. Singh,¹ S. Marik,¹ and R. P. Singh^{1,*}

¹*Department of Physics, Indian Institute of Science Education and Research Bhopal, Bhopal, 462066, India*

(Dated: February 23, 2022)

We report synthesis and properties of superconducting Bi_2PdPt , a new member of Bi-Pd based compounds known for their simultaneous existence of topological surface states and superconductivity. It crystallizes in a hexagonal structure having space group $P6_3/mmc$. A detailed investigation of the properties via transport, magnetization, and specific heat measurements confirm bulk superconductivity with transition temperature, $T_C = 4.0(1)$ K in moderate coupling limit.

I. INTRODUCTION

The topological aspects of electronic states provide a thrust in the latest research of condensed matter physics. With the realization of spin polarization in these electronic states, various exotic quantum phases emerge, such as topological insulator, topological semimetals, and topological superconductor (TSC) [1–3]. Particularly, topological superconductors attracted immense attention due to the potential appearance of exotic quasiparticles called Majorana fermions and their application in topological quantum computing. A topological superconductor is characterized by a bulk superconducting gap and Majorana zero modes at the symmetry protected topological surface states (TSSs) [3]. The various proposed ways to realize TSC include carrier doped topological insulator and superconductor-topological insulator heterostructures [4, 5] which introduce the challenge to prepare high quality samples and observe interfacial phenomena. Bulk compounds where non-trivial band structure and superconductivity intrinsically coexists emerge as a promising route to realize topological superconductivity.

Bi-based materials are known for the presence of TSSs [7–14]. The Bi-based binary systems α -PdBi, α -PdBi₂, and β -PdBi₂ are among the promising bulk topological superconductivity candidates. Notably, in α -PdBi₂ and non-centrosymmetric α -PdBi, Rashba surface states near the Fermi level, E_F were theoretically predicted and experimentally verified via angle-resolved photoemission spectroscopy (ARPES) with intrinsic superconductivity [15–20]. Moreover, the observed non-helical spin texture near E_F for β -PdBi₂ combined with the various reports of fully gapped multiband superconductivity in bulk, suggests the realization of Majorana fermions at the surface states [21–25].

Recently, PtBi₂ displays a large anisotropy for the in-plane and inter-plane transport and is stated as a bulk topological metal with pressure-induced superconductivity at 2.0 K [26, 27]. It indicates that the vast family of Bi compounds is associated with various aspects of topological electronic states and accompanied by supercon-

ductivity, which demands detailed investigation in this family. Further, the spin-orbit coupling (SOC) strength affect the Fermi surface to capture the non-trivial band topology [8, 28] and also impact the low-energy properties like superconductivity [29]. Thus, the superconductivity with high SOC strength and the possible non-trivial band structure may direct unconventional ground state. As SOC is directly proportional to the fourth power of atomic number Z , introducing a heavier element will increase the SOC strength of the system.

We have synthesized a new member of the Bi compound family, Bi_2PdPt , where a Pt atom partially replaces a Pd atom from PdBi. Powder XRD and Laue diffraction were performed to investigate the crystal structure and orientation. The superconducting and normal state properties of Bi_2PdPt studied using transport, magnetization, and specific heat measurements. Type-II superconductivity in moderate coupling limit is established in Bi_2PdPt .

II. EXPERIMENTAL DETAILS

Single-crystal of Bi_2PdPt was prepared by the modified Bridgman method. Firstly, the polycrystalline sample was prepared using the solid-state reaction method by taking a stoichiometric mixture of required elemental powder Bi (99.99%), Pd (99.95%) and Pt (99.9%). The palletized form of the mixture was subsequently heated at 700°C for four days in a vacuum sealed tube, which was then transferred in a conical end quartz ampoule for single-crystal growth. The ampoule dwelled at 700°C for 12 h and slowly cooled up to 650°C at the rate of 0.4°C/hr, followed by the water quenching. The obtained single-crystal is extremely brittle with a metallic lustre. Mechanically cleaved single-crystals were used for all the measurements. Powder x-ray diffraction data for grinded single-crystal was collected at room temperature using PANalytical X'Pert powder diffractometer with CuK_α ($\lambda = 1.5406$ Å) radiation. The Laue diffraction pattern was recorded using the Photonic-Science Laue camera system for single-crystal orientation and quality determination. The magnetic measurements were performed on the vibrating sample magnetometer (VSM) option of

* rpsingh@iiserb.ac.in

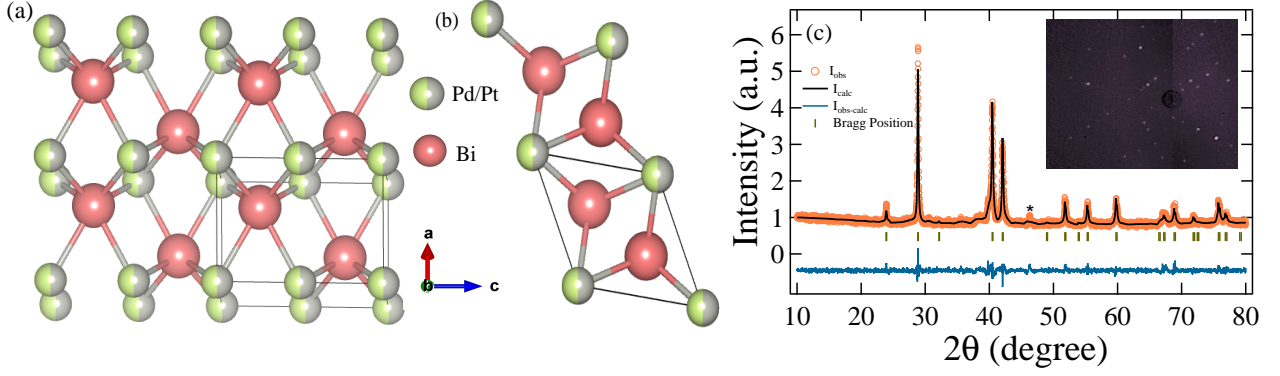


FIG. 1. The NiAs hexagonal crystal structure of Bi_2PdPt is shown with solid orange ball as Bi atoms and half green or grey solid ball as Pd/Pt atoms. (a) Shows the side view of the crystal structure and (b) shows the top view. (c) Rietveld refined pattern, represented by black line, of XRD recorded at room temperature (orange open circle) for Bi_2PdPt is shown. Inset shows the Laue diffraction pattern of the single-crystal.

the Quantum Design Magnetic Property Measurement System (MPMS-3). AC transport and specific heat measurements with two- τ relaxation method were performed using Quantum Design Physical Property Measurement System (PPMS) 9 T with an applied magnetic field parallel to the crystallographic [001] axis.

III. RESULTS AND DISCUSSION

a. Sample characterization

Rietveld refinement of powder x-ray diffraction pattern of Bi_2PdPt was performed using FullProf software (shown in Fig. 1) [30]. A small elemental impurity peak of Pt is observed shown by an asterisk in the Fig. 1. The refinement confirms the crystallization of Bi_2PdPt in NiAs hexagonal crystal structure having space group $P6_3/mmc$, which is different from the structures reported for other superconducting compounds of the family, α - BiPd (non-centrosymmetric) and α -, β - PdBi_2 , PtBi_2 (layered structure) [15, 19, 23, 26].

The structure of Bi_2PdPt consists of Bi atoms that lie inside the hexagonal geometry while Pd and Pt atoms share the edges sites with equal probability, as shown in the Fig. 1(a) and (b). Detailed refinement results with the associated Wyckoff position of each atom are summarized in Table I. The Laue diffraction pattern of different crystals of the same batch depicts the orientation of the crystal along [001] direction, and bright spots tell the quality of the single-crystal as shown in the inset of Fig. 1(c).

b. Superconducting and normal state properties

In-plane AC resistivity at zero magnetic field in temperature range, 1.8 K to 250 K, was measured for single-

TABLE I. Structure parameters of Bi_2PdPt obtained from the Rietveld refinement of XRD

Structure		Hexagonal			
Space group		$P6_3/mmc$			
Lattice parameters					
a = b (Å)		4.294(5)			
c (Å)		5.567(1)			
Atom	Wyckoff position	x	y	z	Occupancy
Bi	2c	0.333	0.666	0.250	0.0839
Pd	2a	0	0	0	0.0417
Pt	2a	0	0	0	0.0416

crystal of Bi_2PdPt , as shown in Fig. 2. A sharp resistivity drop from the normal state resistivity at $T_{C,onset} = 4.0(1)$ K with the width of 0.1 K is registered as a superconducting transition. Above transition temperature resistivity behaviour of Bi_2PdPt shows slight deviation from linear behaviour, which is described by Wilson's theory [31]. However, the high value of absolute resistivity with a saturated trend is allied with α - BiPd and other A-15 compounds where a parallel resistor model is implanted [32]. The resistivity behaviour for Bi_2PdPt is characterised using parallel resistor model described by Wisemann as [33],

$$\frac{1}{\rho(T)} = \frac{1}{\rho_s} + \frac{1}{\rho_i(T)} \quad (1)$$

where ρ_s is saturated resistivity independent of the temperature and $\rho_i(T)$ is the ideal contribution consisting two terms which expressed as,

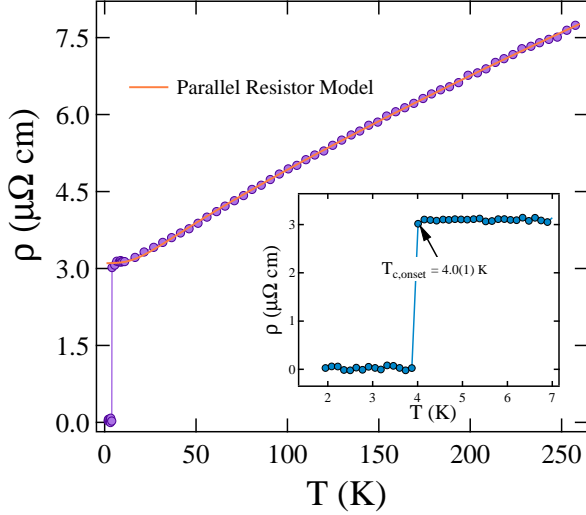


FIG. 2. Temperature dependence of resistivity in zero field fitted using the parallel resistor model above transition temperature is shown in main panel. The inset shows the limited temperature region showing superconducting transition at $T_{C,onset} = 4.0(1)$ K.

$$\rho_i(T) = \rho_{i,0} + C \left(\frac{T}{\Theta_R} \right)^n \int_0^{\Theta_R/T} \frac{x^n}{(e^x - 1)(1 - e^{-x})} dx \quad (2)$$

here the first term $\rho_{i,0}$ is temperature-independent residual resistivity, and the second term represents the temperature dependent contribution including the effect of electron-phonon scattering stated by the generalized Bloch-Grüneisen expression [31, 34]. Θ_R is the Debye temperature from resistivity measurement, and C is a material-dependent quantity. Best fitting of Bi_2PdPt for $n = 3$ yields Debye temperature, $\Theta_R = 123(3)$ K, $C = 5.70(2) \mu\Omega\text{-cm}$, $\rho_s = 47(3) \mu\Omega\text{-cm}$ and $\rho_{i,0} = 3.32(1) \mu\Omega\text{-cm}$. The estimated residual resistivity ratio, $\rho(250\text{K})/\rho(5\text{K}) = 2.5$ is much smaller than the reported values for the other Bi-Pd compounds, which can be possibly due to the increase in disorder of the system by Pt presence [32, 35].

Magnetization versus temperature measurement at 1 mT magnetic field in zero-field-cooled warming (ZFCW) and field-cooled cooling (FCC) mode is shown in Fig. 3(a). Curve shows a diamagnetic onset at temperature $T_C = 3.98(1)$ K perpendicular to crystallographic [001] axis of single-crystalline Bi_2PdPt . The poor overlapping of the ZFCW and FCC curve depicts the presence of a strong pinning centre in the sample with superconducting volume fraction close to 96% certain the bulk property. Magnetization hysteresis loop under an applied magnetic field of ± 1 T at temperature, 1.8 K is shown in Fig. 3(b).

The loop represents the conventional type-II behaviour along with an irreversible nature of magnetization below $H_{irr} = 0.45$ T, above which unpinning of the vortices start taking place.

Further, to estimate the lower critical field value H_{C1} , the magnetization variation in the applied magnetic field at different isotherms up to transition temperature, T_C , were analyzed. H_{C1} for each isotherm is considered as a magnetic field value where the curve starts to deviate from the linear Meissner state, as shown in Fig. 3(c). The temperature evolution of the lower critical field is fitted with the Ginzburg-Landau (GL) equation,

$$H_{C1}(T) = H_{C1}(0) \left[1 - \left(\frac{T}{T_C} \right)^2 \right] \quad (3)$$

which gives $H_{C1}(0) = 2.96(4)$ mT for $T_C = 3.98(1)$ K (Fig. 3(d)). The upper critical field H_{C2} is evaluated by the observed shifts in superconducting transition temperature with the increasing applied magnetic field. The shift in the transition temperature, T_C is marked from magnetization at onset and for resistivity measurements at 90% drop from normal state resistivity value ($T_{C,90\%}$), as shown in the inset of Fig. 4. The upper critical field $H_{C2}(0)$ is estimated from the expression,

$$H_{C2}(T) = H_{C2}(0) \left[\frac{(1 - t^2)}{(1 + t^2)} \right] \quad (4)$$

here $t = T/T_C$, reduced temperature. The fitted data yields $H_{C2,M}(0) = 0.92(1)$ T and $H_{C2,\rho}(0) = 1.08(1)$

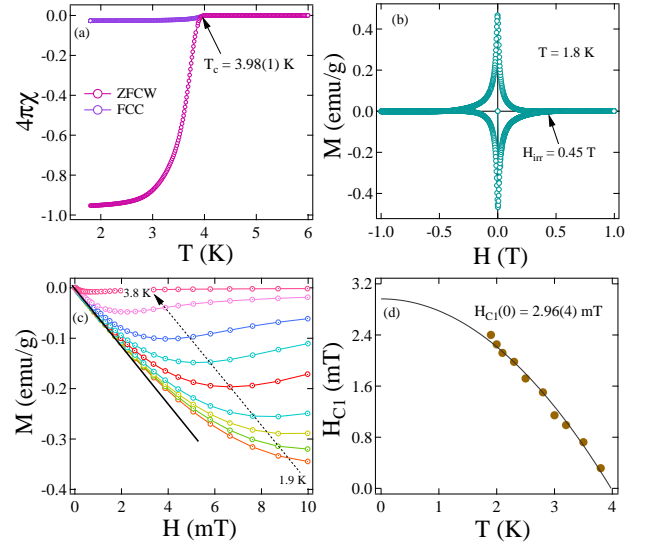


FIG. 3. a) Shows the superconducting transition in 1 mT magnetic field at $T_{c,onset} = 3.98(1)$ K. (b) Magnetization hysteresis loop at 1.8 K. (c) Magnetic moment variation under magnetic field at different temperature upto transition temperature. (d) Lower critical field with temperature fitting using GL equation Eq. (4).

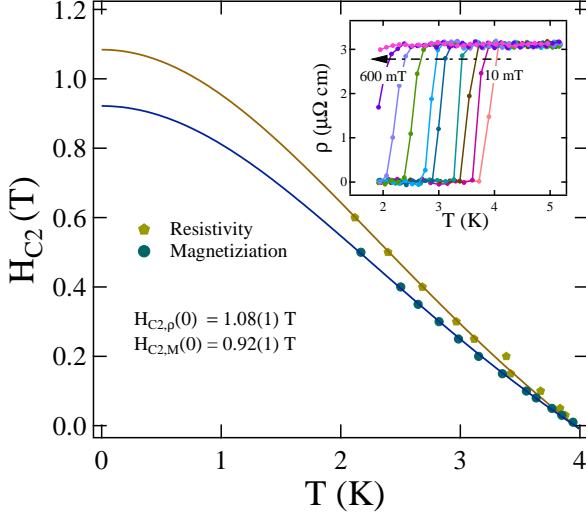


FIG. 4. The upper critical field variation with temperature is determined via magnetization and resistivity measurements and fitted by using the equation Eq. (4) is shown. Inset shows the resistivity drop temperature variation with applied magnetic field.

T from magnetization, and resistivity measurements, respectively displayed in Fig. 4.

In addition to the resistivity and magnetization measurements, specific heat is also measured at zero field and 2 T (well above the upper critical field) under temperature variation, shown in Fig. 5. A small anomaly in 0 T specific heat measurement is inscribed around 3.93(7) K, as shown in the inset of Fig. 5, which is in allied with the superconducting transition temperature recorded from resistivity and magnetization measurements. Whereas the measurement recorded at 2 T presents the normal state of Bi₂PdPt. The normal state specific data is fitted using the Debye relation,

$$C = \gamma_n T + \beta_3 T^3 + \beta_5 T^5 \quad (5)$$

where γ_n is Sommerfeld coefficient corresponding to electronic contribution, β_3 Debye constant represents phononic contribution, and β_5 produces the anharmonic contribution to the specific heat. The fitted data produces $\gamma_n = 5.1(6)$ mJmol⁻¹K⁻², $\beta_3 = 1.72(6)$ mJmol⁻¹K⁻⁴ and $\beta_5 = 11.2(1)$ μ Jmol⁻¹K⁻⁶ (Fig. 5). The Sommerfeld coefficient value matches well with the α -PdBi reported value, but a large deviation from α - and β -PdBi₂ is observed [32, 35, 36]. According to the free-electron theory, the Sommerfeld coefficient is used to evaluate the density of state at Fermi level as per the relation $\gamma_n = \left(\frac{\pi^2 k_B^2}{3}\right) D_C(E_F)$, where $k_B = 1.38 \times 10^{-23}$ J K⁻¹ is Boltzmann constant. The $D_C(E_F)$ is calculated to be 2.1(2) states eV⁻¹ f.u.⁻¹. Further, considering the Debye model, the Debye temperature Θ_D is estimated to

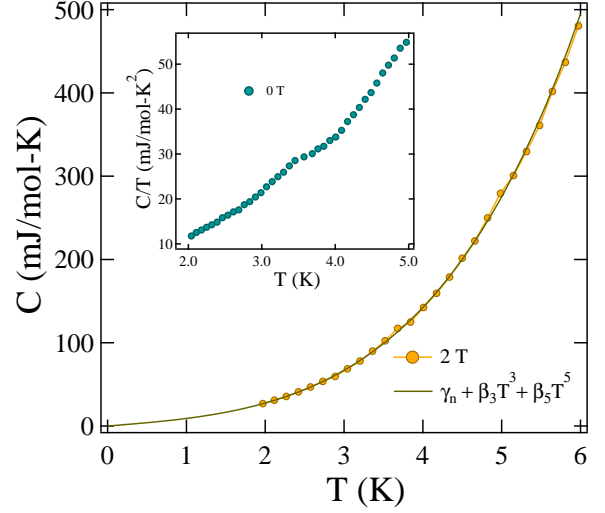


FIG. 5. The temperature dependence specific heat of the Bi₂PdPt represented in C vs T form at 2 T magnetic field is fitted with the equation Eq. (5). Inset shows the C vs T curve at zero magnetic field curve where anomaly is clearly observed.

be 165(2) K for $\beta_3 = 1.72(6)$ mJ mol⁻¹ K⁻⁴ using the expression $\theta_D = \left(\frac{12\pi^4 R N}{5\beta_3}\right)^{\frac{1}{3}}$, where $R = 8.314$ J mol⁻¹K⁻¹ is a gas constant. The calculated Debye temperature value is consistent with the value obtained from parallel resistor model. The average electron-phonon coupling constant, λ_{e-ph} is calculated by implanting McMillan's theory given as [37],

$$\lambda_{e-ph} = \frac{1.04 + \mu^* \ln(\theta_D/1.45T_C)}{(1 - 0.62\mu^*) \ln(\theta_D/1.45T_C) - 1.04} \quad (6)$$

where μ^* varies in the range of $0.1 \leq \mu^* \leq 0.15$, a material-specific value accounts for screened Coulomb repulsion. Considering $T_C = 3.93(7)$ K, $\theta_D = 165(2)$ K and $\mu^* = 0.1$ (as speculate for Bi-Pd binary compounds) obtained $\lambda_{e-ph} = 0.64(1)$, which puts Bi₂PdPt in the moderately coupled superconductor regime respective to other Bi-Pd compounds α -, β -PdBi₂, and α -PdBi [32, 36].

c. Superconducting parameters and Uemura Plot

The external applied magnetic field puts a limiting field on the superconductor, portrayed independently by spin paramagnetic and orbital limiting effects. According to the BCS theory, spin paramagnetic effect comes from pairing breaking due to Zeeman effect defined as the Pauli limiting field, $H_{C2}^P(0) = 1.86 T_C$ [38, 39]. For Bi₂PdPt with $T_C = 3.98(1)$ K, yields $H_{C2}^P(0) = 7.40(2)$ T. The orbital limit for an upper critical field refers to the critical field where vortex cores begin to overlap.

The orbital limiting field is given by Werthamer-Helfand-Hohenberg (WHH) expression [40, 41],

$$H_{C2}^{orbital}(0) = -\alpha T_C \left. \frac{dH_{C2}(T)}{dT} \right|_{T=T_C} \quad (7)$$

where $\alpha = 0.69$ for dirty limit and 0.73 for clean limit superconductors. The initial slope $\left. \frac{dH_{C2}(T)}{dT} \right|_{T=T_C}$ at $T = T_C$ is estimated to be 0.23(1) T/K which gives $H_{C2}^{orbital}(0) = 0.64(1)$ T considering the dirty limit. Moreover, the relative strength of Pauli and orbital limiting field is measured by Maki parameter defined by the relation $\alpha_M = \sqrt{2}H_{C2}^{orb}(0)/H_{C2}^P(0)$, evaluates $\alpha_M = 0.12(2)$ [42]. The small value of Maki parameter indicates the negligible effect of Pauli limiting field for Bi₂PdPt.

Further, the fundamental superconducting length parameters is calculated from upper, $H_{C2}(0)$, and lower, $H_{C1}(0)$ critical field values. The Ginzburg-Landau coherence length ($\xi_{GL}(0)$) is estimated from $\xi_{GL}(0) = \sqrt{\frac{\Phi_0}{2\pi H_{C2}(0)}}$ [43], here $\Phi_0 = 2.07 \times 10^{-15}$ Tm² is the magnetic flux quantum. Using $H_{C2,M}(0) = 0.92(1)$ T, $\xi_{GL}(0)$ is evaluated to be 190(1) Å. The equation [44],

$$H_{C1}(0) = \frac{\Phi_0}{4\pi\lambda_{GL}^2(0)} \left(\ln \frac{\lambda_{GL}(0)}{\xi_{GL}(0)} + 0.12 \right) \quad (8)$$

provides the Ginzburg-Landau penetration depth, $\lambda_{GL}(0) = 4231(76)$ Å for $H_{C1}(0) = 2.96(4)$ mT and $\xi_{GL}(0) = 190(1)$ Å. Moreover, the ratio $\frac{\lambda_{GL}(0)}{\xi_{GL}(0)}$ gives the Ginzburg-Landau parameter, $\kappa_{GL} = 22.2(5)$ which is much greater than $1/\sqrt{2}$ indicating a strong type-II superconductivity in Bi₂PdPt. The thermodynamic critical field H_C , is evaluated by using the expression [44]; $H_{C1}(0)H_{C2}(0) = H_C^2 \ln \kappa_{GL}$, yielding $H_C = 29(1)$ mT.

For Bi₂PdPt, in order to determine the rest of the superconducting parameters including London penetration depth λ_L , electronic mean free path l_e and to verify dirty limit superconductivity, a set of equation is used assuming the spherical Fermi surface. The electronic mean free path, l_e is estimated from the quasiparticle number density, n and Sommerfeld coefficient, γ_n . The quasiparticle number density of Bi₂PdPt has been extracted from Hall measurement, $n = 2.45(2) \times 10^{28}$ m⁻³ (more details in appendix). The Fermi vector, k_F is evaluated using $k_F = (3\pi^2 n)^{1/3}$, which gives $k_F = 0.90(1)$ Å⁻¹. The effective mass, m^* is calculated from Sommerfeld coefficient, $m^* = (\hbar k_F)^2 \gamma_n / \pi^2 n k_B^2$. For k_B is Boltzmann constant and $\gamma_n = 95.51$ J m⁻³ K⁻², $m^* = 2.0(3) m_e$. According to Drude Model [43], Fermi velocity is determined from the relation $v_F = \hbar k_F / m^* = 5.1(7) \times 10^5$ m s⁻¹ and scattering time from $\tau^{-1} = ne^2 \rho_0 / m^*$, which further used to calculate electronic mean free path, $l_e = v_F \tau$ providing $l_e = 455(68)$ Å.

In consideration of BCS theory, the coherence length ξ_0 is defined as $0.18 \hbar v_F / k_B T_C$ providing $\xi_0 = 1756(147)$

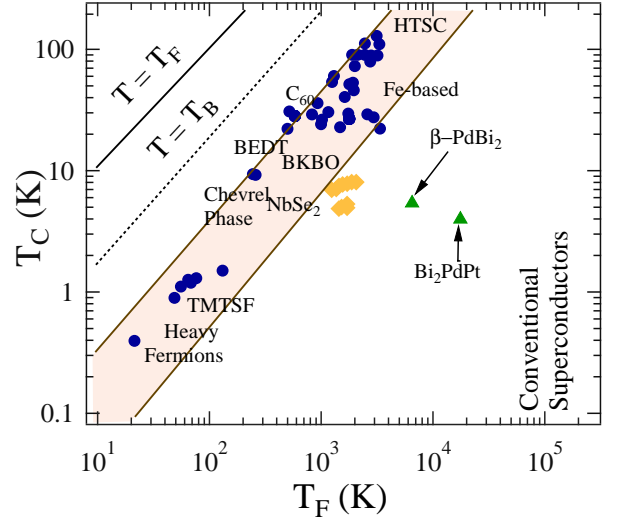


FIG. 6. The Uemura plot showing the superconducting transition temperature T_C vs the effective Fermi temperature T_F for Bi₂PdPt with β -PdBi₂, shown as solid green circle. Other data points represent the different families of superconductors together with the shaded region representing the families of unconventional superconductors. The dashed line corresponds to the Bose-Einstein condensation temperature T_B .

Å. The ratio of $\xi_0/l_e = 3.9$ is greater than 1, implying Bi₂PdPt is a dirty limit superconductor. Further in the dirty limit, the London penetration depth λ_L [45], is written as,

$$\lambda_L = \left(\frac{m^*}{\mu_0 n e^2} \right)^{1/2}. \quad (9)$$

From the above expression the estimated λ_L is 483(36) Å. The order of calculated parameters matches well with β -PdBi₂ where dirty limit superconductivity is observed [24] whereas α -PdBi lies in a clean type-II superconducting limit [32].

Moreover, to classify the Bi₂PdPt in the context of other superconductors, Uemura plot [46] of T_C with effective Fermi temperature, T_F has been plotted, which is used to define the character of unconventionality of a superconductor based on the ratio of $\frac{T_C}{T_F}$. For 3D spherical Fermi surface, Fermi temperature is calculated using [47],

$$k_B T_F = \frac{\hbar^2}{2} (3\pi^2)^{2/3} \frac{n^{2/3}}{m^*}, \quad (10)$$

where n is the quasiparticle number density per unit volume, and m^* is the effective mass of quasiparticles. The T_F value is estimated to be $T_F = 17576(104)$ K, by considering the respective values of parameters from Table II. The ratio $\frac{T_C}{T_F} = 0.0002$ places this material,

TABLE II. Parameters in the superconducting and normal state of Bi₂PdPt and α -BiPd

Parameters	Unit	Bi ₂ PdPt	α -BiPd [32]
T_C	K	4.0	3.8
$H_{C1}(0)$	mT	2.96	12.0
$H_{C2,M}(0)$	T	0.92	0.8
$H_{C2}^P(0)$	T	7.40	7.07
$H_{C2}^{Orb}(0)$	T	0.64	
$\xi_{GL}(0)$	Å	190	170
$\lambda_{GL}(0)$	Å	4231	1792
k_{GL}		22.2	7.6
γ_n	mJ mol ⁻¹ K ⁻²	5.1	4.0
θ_D	K	165.0	169.0
ξ_0/l_e		3.9	0.01
v_F	10 ⁵ m s ⁻¹	5.1	
n	10 ²⁸ m ⁻³	2.45	
T_F	K	17576	
m^*/m_e		2.0	

Bi₂PdPt close to other family member, β -PdBi₂ and outside the band of unconventional superconductor which includes iron based superconductors, cuprates and Chevrel phase [48, 49]. The conventional superconductors are considered to be on the right-hand side of the Uemura plot. Bi₂PdPt with the other member of the Bi-Pd compound family, β -PdBi₂ [24] are shown by the solid green symbol in Fig. 6.

Among the Bi-Pd compound family, Bi₂PdPt is the highest possible SOC strength candidate, based on the presence of heavy constituent elements, establishes a strong foundation to exhibit intriguing properties. The different crystal structure NiAs type of Bi₂PdPt eliminates all the possibilities of any secondary superconducting phase presence of Bi-Pd/Pt compound, implementing the intrinsic bulk superconductivity. Hall measurement (see appendix) suggests dominated hole charge carries (10²⁸m⁻³) same as for other Bi-Pd compounds, which indicate a very low effect in the electronic state with the Pt presence. The specific heat of Bi₂PdPt gives Sommerfeld coefficient 5.1(6) mJmol⁻¹K⁻², which is slightly greater than what is reported for α -BiPd, suggests only a minimal increase in density of states at E_F . However, the observed value is comparable to that of β -PdBi₂ and Pt_{1.26}Bi₂ [50]. Concluding neither substitution at Pd site nor increasing the Bi concentration predominately affects the density of states in Bi-Pd/Pt compounds. Despite the presence of heavy 5d Pt element, no change in phonon frequency, extracted from Debye temperature, is noted between Bi₂PdPt and α -BiPd [32].

Moreover, the bulk measurement of Bi₂PdPt is not sufficient to establish the gap symmetry of the sample. The possible explanation of low specific jump value can be due to multiband superconductivity with a single supercon-

ducting gap [51]. The layered transition metal dichalcogenide superconductors have been well known to exhibit no anomaly in specific heat measurement [52]. In addition, the low value of specific heat jump or no jump at all is also observed in many Bi-based half Heusler alloys (RPdBi), where superconductivity is attributed to the surface states [53]. Further, the similar behaviour is determined for the case of strongly or locally disordered systems such as quasi-skutterudites [54].

No deviation or anisotropy has been observed in the upper critical field of Bi₂PdPt, directing towards the bulk nature of the superconducting state and absence of multi-gap superconductivity. Apart from this, the variation of superconducting volume fraction with the different cooling procedures of sample preparation showed the grain boundaries effect in the sample (details in appendix). To fully understand the effect of increased SOC strength, the possible reason for the low value of specific heat jump and address any non-trivial band structure in the normal state of Bi₂PdPt detailed theoretical and experimental analysis of the superconducting ground state with band topology is required.

IV. CONCLUSION

In summary, we synthesized the single-crystalline Bi₂PdPt and transport, magnetization, and specific heat measurements performed for detailed analysis of superconducting properties. The superconducting transition of Bi₂PdPt has been reported at 4.0(1) K with upper and lower critical field value, $H_{C1} = 2.96(4)$ mT and $H_{C2,M} = 0.92(1)$ T, fitted using Ginzburg-Landau equation. An anomaly was observed around transition temperature in specific heat measurement confirms the bulk superconductivity. The comparison of various normal and superconducting state parameters of Bi₂PdPt and α -BiPd have been summarized in Table II. The Bi₂PdPt is classified as a moderately coupled type-II dirty limit superconductor. The estimated value of Fermi temperature, T_F places Bi₂PdPt close to the other member of the family, β -PdBi₂. Further microscopic measurements such as muon spectroscopy, scanning tunnelling microscope (STM), and angle-resolved photoemission spectroscopy (ARPES) are required to understand the superconducting ground state and the possible topological nature of Bi₂PdPt.

V. ACKNOWLEDGMENTS

A. Kataria acknowledges the funding agency Council of Scientific and Industrial Research (CSIR), Government of India, for providing SRF fellowship (Award No: 09/1020(0172)/2019-EMR-I). R. P. S. acknowledges Science and Engineering Research Board, Government of India for the Core Research Grant CRG/2019/001028.

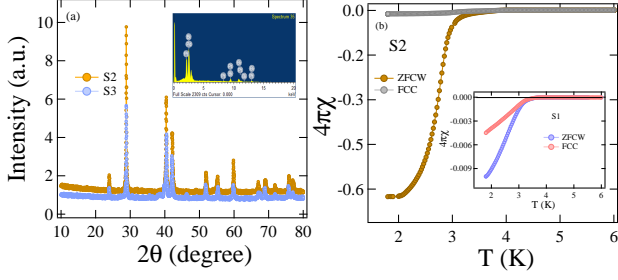


FIG. 7. (a) Shows the XRD comparison of powder sample having two different cooling rate 0.5°C/hr (S2) and 0.4°C/hr (S3) while preparation, with the inset shows the EDS pattern of S3 sample. (b) Shows the magnetic measurement compilation of S2 and S1 in the inset, whereas S3 is shown in Fig. 3(a).

VI. APPENDIX

a. Characterization

Superconducting volume fraction in Bi_2PdPt is highly dependent on the sample cooling procedure during preparation. Three different samples made, such as S1, cooled at 1.0°C/hr , S2 cooled at 0.5°C/hr , and S3 cooled at 0.4°C/hr while preparing the sample. XRD of the two samples S2 and S3 is shown in Fig. 7(a). The composition of one of the samples extracted from energy dispersive spectroscopy (EDS) is also shown in the inset of Fig. 7 (a), clearly indicating the Pt presence. The results from the magnetic characterization of S1 and S2 are presented in Fig. 7(b). The observed superconducting transition temperature is the same for all three samples; however superconducting shielding fraction 96% is the maximum for S3. S2 only shows 60% volume fraction with less than 10% fraction is observed in S1, implying samples cooled only at a specific rate show a large volume fraction with the same diamagnetic onset temperature in magnetization measurement. Thus, reflecting the effect on grain boundaries and point defects of samples due to different cooling procedures [55].

b. Normal state properties

To perceive the normal state properties of Bi_2PdPt , magnetoresistance (MR) and normal hall effect were also measured. The hall measurements were done on Bi_2PdPt under varying magnetic field of ± 9 T at 30 K to extract the carrier density as shown in the left panel of Fig. 8(a), where a linear variation with magnetic field represents the small contribution from the longitudinal resistivity. The hall coefficient, R_H , was determined by the slope of the variation ρ_{xy} with both $+H$ and $-H$ fields. The estimated $R_H = 2.52(2) \times 10^{-4} \text{ cm}^3/\text{C}$, and the positive sign indicate the hole as the dominant charge carrier

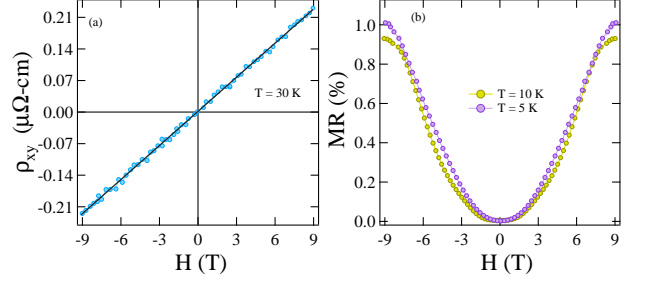


FIG. 8. (a) Hall resistivity at $T = 30$ K under field variation of ± 9 T. (b) Represent the MR data taken at $T = 5$ K and $T = 10$ K on Bi_2PdPt crystal.

in the sample. By simply using the single band expression $n = 1/R_H q$, the electron concentrations was calculated, $n = 2.45(2) \times 10^{28} \text{ m}^{-3}$. The carrier density order matches with the other reported for $\alpha\text{-PdBi}$ and PdBi_2 [56]. MR was measured in the longitudinal configuration under a varying magnetic field of 9 T at different temperatures. MR with magnetic field dependence is defined as $\frac{\rho_{xx}(H) - \rho_{xx}(0)}{\rho_{xx}(0)}$. A significant small MR value is observed in our sample Fig. 8(b).

-
- [1] A. P. Schnyder, S. Ryu, A. Furusaki, and A. W. W. Ludwig, Phys. Rev. B 78, 195125 (2008).
 - [2] X. L. Qi, T. L. Hughes, S. Raghu, and S.C. Zhang, Phys. Rev. Lett. 102, 187001 (2009).
 - [3] X. L. Qi and S.C. Zhang, Rev. Mod. Phys. 83, 1057 (2011).
 - [4] M. Sato, and Y. Ando, Reports on Progress in Phys. 80, 076501 (2017).
 - [5] L. Fu and C. L. Kane, Phys. Rev. Lett. 100, 096407 (2008).
 - [6] A. Yu. Kitaev, Physics-uspekhi 44, 131 (2001).
 - [7] L. Fu, and C. L. Kane, Phys. Rev. B 76, 045302 (2007).
 - [8] H. Zhang, C. X. Liu, X. L. Qi, X. Dai, Z. Fang, and S. C. Zhang, Nature Physics, 5, 438 (2009).
 - [9] T. Sato, K. Segawa, H. Guo, K. Sugawara, S. Souma, T. Takahashi, and Y. Ando, Phys. Rev. Lett. 105, 136802 (2010).
 - [10] K. Kuroda, M. Ye, A. Kimura, S. V. Ereemeev, E. E. Krasovskii, E. V. Chulkov, Y. Ueda, K. Miyamoto, T. Okuda, K. Shimada, H. Namatame, and M. Taniguchi, Phys. Rev. Lett. 105, 146801 (2010).
 - [11] Y. L. Chen, Z. K. Liu, J. G. Analytis, J.-H. Chu, H. J. Zhang, B. H. Yan, S.-K. Mo, R. G. Moore, D. H. Lu, I. R. Fisher, S. C. Zhang, Z. Hussain, and Z.-X. Shen, Phys. Rev. Lett. 105, 266401 (2010).
 - [12] S. Souma, K. Eto, M. Nomura, K. Nakayama, T. Sato, T. Takahashi, K. Segawa, and Y. Ando, Phys. Rev. Lett. 108, 116801 (2012).
 - [13] K. Kuroda, H. Miyahara, M. Ye, S. V. Ereemeev, Yu. M. Koroteev, E. E. Krasovskii, E. V. Chulkov, S. Hiramoto, C. Moriyoshi, Y. Kuroiwa, K. Miyamoto, T. Okuda, M. Arita, K. Shimada, H. Namatame, M. Taniguchi, Y. Ueda, and A. Kimura, Phys. Rev. Lett. 108, 206803 (2012).

- (2012).
- [14] Y. Nakajima, R. Hu, K. Kirshenbaum, A. Hughes, P. Syers, X. Wang, and J. Paglione, *Science advances* 1, e1500242 (2015).
 - [15] Y. Zhou, X. Chen, C. An, Y. Zhou, L. Ling, J. Yang, C. Chen, L. Zhang, M. Tian, Z. Zhang, and Z. Yang, *Phys. Rev. B* 99, 054501 (2019).
 - [16] S. Mitra, K. Okawa, S. K. Sudheesh, T. Sasagawa, Jian-Xin Zhu, and Elbert E. M. Chia, *Phys. Rev. B* 95, 134519 (2017).
 - [17] K. Dimitri, M. M. Hosen, G. Dhakal, H. Choi, F. Kabir, C. Sims, D. Kaczorowski, T. Durakiewicz, J.X. Zhu, and M. Neupane, *Phys. Rev. B* 97, 144514 (2018).
 - [18] H. Choi, M. Neupane, T. Sasagawa, Elbert E. M. Chia, and J. X. Zhu, *Phys. Rev. M* 1, 034201 (2017).
 - [19] Z. Sun, M. Enayat, A. Maldonado, C. Lithgow, E. Yelland, D. Peets, D. C. Peets, A. Yaresko, A. P. Schnyder, and P. Wahl, *Nat. Commun.* 6, 1 (2015).
 - [20] A. Yaresko, A. P. Schnyder, H. M. Benia, C.M. Yim, G. Levy, A. Damascelli, C. R. Ast, D. C. Peets, and P. Wahl, *Phys. Rev. B* 97, 075108 (2018).
 - [21] M. Sakano, K. Okawa, M. Kanou, H. Sanjo, T. Okuda, T. Sasagawa and K. Ishizaka, *Nat. Commun.* 6, 8595 (2015).
 - [22] T. Xu, B. T. Wang, M. Wang, Q. Jiang, X. P. Shen, B. Gao, M. Ye, and S. Qiao, *Phys. Rev. B* 100, 161109(R) (2019).
 - [23] J. Kacmarcik, Z. Pribulova, T. Samuely, P. Szabo, V. Cambel, J. Soltys, E. Herrera, H. Suderow, A. Correa-Orellana, D. Prabhakaran, and P. Samuely, *Phys. Rev. B*, 93, 144502 (2016).
 - [24] P. K. Biswas, D. G. Mazzone, R. Sibille, E. Pomjakushina, K. Conder, H. Luetkens, C. Baines, J. L. Gavilano, M. Kenzelmann, A. Amato, and E. Morenzoni, *Phys. Rev. B* 93, 220504(R) (2016).
 - [25] E. Herrera, I. Guillamon, J. A. Galvis, A. Correa, A. Fente, R. F. Luccas, F. J. Mompean, M. Garcia-Hernandez, S. Vieira, J. P. Brison, and H. Suderow, *Phys. Rev. B* 92, 054507 (2015).
 - [26] C. Q. Xu, X. Z. Xing, Xiaofeng Xu, Bin Li, B. Chen, L. Q. Che, Xin Lu, Jianhui Dai, and Z. X. Shi, *Phys. Rev. B* 94, 165119 (2016).
 - [27] J. Wang, X. Chen, Y. Zhou, C. An, Y. Zhou, C. Gu, M. Tian, and Z. Yang, *Phys. Rev. B* 103, 014507 (2021).
 - [28] M.Z. Hasan, and C. L. Kane, *Rev. Mod. Phys.* 82(4), 3045 (2010).
 - [29] D.F. Shao, X. Luo, W. J. Lu, L. Hu, X. D. Zhu, W. H. Song, X. B. Zhu, and Y. P. Sun. *Scientific Reports* 6, 1 (2016).
 - [30] J. Rodr  guez-Carvajal, *Phys. B: Cond. Matt.* 192, 55 (1993).
 - [31] A. H. Wilson, *Theory of Metals* (Cambridge University Press, Cambridge, England, 1958).
 - [32] B. Joshi, A. Thamizhavel, and S. Ramakrishnan, *Phys. Rev. B* 84, 064518 (2011).
 - [33] H. Wiesmann, M. Gurvitch, H. Lutz, A. K. Ghosh, B. Schwarz, M. Strongin, P. B. Allen, and J.W. Halley, *Phys. Rev. Lett.* 38, 782 (1977).
 - [34] G. Grimvall, *The Electron-Phonon Interaction in Metals* (North-Holland, Amsterdam, 1981).
 - [35] Y. Imai, F. Nabeshima, T. Yoshinaka, K. Miyatani, R. Kondo, S., Komiya, I. Tsukada, and A. Maeda, *Jour. of the Phys. Soc. of Jap.* 81, 113708 (2012).
 - [36] G. Pristas, Mat. Orendac, S. Gabani, J. Kacmarcik, E. Gazo, Z. Pribulova, A. Correa-Orellana, E. Herrera, H. Suderow, and P. Samuely, *Phys. Rev. B* 97, 134505 (2018).
 - [37] W. L. McMillan, *Phys. Rev.* 167, 331 (1968).
 - [38] B. S. Chandrasekhar, *Appl. Phys. Lett.* 1, 7 (1962).
 - [39] A. M. Clogston, *Phys. Rev. Lett.* 9, 266 (1962).
 - [40] E. Helfand, and N. R. Werthamer, *Phys. Rev.* 147, 288 (1966).
 - [41] N. R. Werthamer, E. Helfand, and P. C. Hohenberg, *Phys. Rev.* 147, 295 (1966).
 - [42] K. Maki, *Phys. Rev. B* 148, 362 (1966).
 - [43] M. Tinkham, *Introduction to Superconductivity*, 2nd ed. (McGraw-Hill, New York, 1996).
 - [44] T. Klimczuk, F. Ronning, V. Sidorov, R. J. Cava, and J.D. Thompson, *Phys. Rev. Lett.* 99, 257004 (2007).
 - [45] D. A. Mayoh, J. A. T Barker, R. P. Singh, G. Balakrishnan, D. McK. Paul, and M. R. Lees, *Phys. Rev. B* 96, 064521 (2017).
 - [46] Y. J. Uemura, G. M. Luke, B. J. Sternlieb, J. H. Brewer, J. F. Carolan, W. N. Hardy, R. Kadono, J. R. Kempton, R. F. Kiefl, S. R. Kreitzman, P. Mulhern, T. M. Riseman, D. L. Williams, B. X. Yang, S. Uchida, H. Takagi, J. Gopalakrishnan, A. W. Sleight, M. A. Subramanian, C. L. Chien, M. Z. Cieplak, G. Xiao, V. Y. Lee, B. W. Statt, C. E. Stronach, W. J. Kossler, and X. H. Yu, *Phys. Rev. Lett.* 62, 2317 (1989).
 - [47] A. D. Hillier and R. Cywinski, *Appl. Magn. Reson.* 13, 95 (1997).
 - [48] K. Hashimoto, K. Cho, T. Shibauchi, S. Kasahara, Y. Mizukami, R. Katsumata, Y. Tsuruhara, T. Terashima, H. Ikeda, M. A. Tanatar, H. Kitano, N. Salovich, R. W. Giannetta, P. Walmsley, A. Carrington, R. Prozorov, and Y. Matsuda, *Science* 336, 1554 (2012).
 - [49] R. Khasanov, H. Luetkens, A. Amato, H. H. Klauss, Z. A. Ren, J. Yang, W. Lu, and Z. X. Zhao, *Phys. Rev. B* 78, 092506 (2008).
 - [50] K. Kudo, H. Y. Nguyen, C. Oh, K. Takaki, and M. No-hara, *Jour. of the Phys. Soc. of Jap.* 90, 063706 (2021).
 - [51] E. Herrera, I. Guillamon, J. A. Galvis, A. Correa, A. Fente, R. F. Luccas, F. J. Mompean, M. Garcia-Hernandez, S. Vieira, J. P. Brison, and H. Suderow, *Phys. Rev. B* 92, 054507 (2015).
 - [52] M. Mandal, M. and R. P. Singh, R.P, *Jour. of Phys. Cond. Matt.* 33, 135602 (2021).
 - [53] P. Orest, D. Kaczorowski, and P. Wisniewski. *Scientific Reports* 5, 1 (2015).
 - [54] A. Slebarski, M. M. Maska, M. Fijalkowski, C. A. McElroy, and M. B. Maple, *Jour. Alloys Comp.* 646, 866 (2015).
 - [55] W. Liu , S. Li, H. Wu , N. Dhale, P. Koirala, and B. Lv, *Phys. Rev. M* 5, 014802 (2021).
 - [56] K. Zhao, B. Lv, Y. Y. Xue, X. Y. Zhu, L. Z. Deng, Z. Wu, and C. W. Chu, *Phys. Rev. B* 92, 174404 (2015).